Dye-Conjugated Spinach RNA by Genetic Alphabet Expansion

RESEARCH ARTICLE

Dye-Conjugated Spinach RNA by Genetic Alphabet Expansion

Kyung Hyun Lee,[a] Michiko Kimoto,[a] Gota Kawai,[b] Itaru Okamoto,[a] Andrea Fin,[a] and Ichiro Hirao*[a]

[a] Dr. K. H. Lee, Dr. M. Kimoto, Dr. I. Okamoto, Dr. A. Fin, Dr. I. Hirao
Institute of Bioengineering and Bioimaging, A*STAR
31 Biopolis Way, The Nanos #07-01, Singapore 138669
E-mail: ichiro@ibb.a-star.edu.sg
[b] Prof. G. Kawai
Chiba Institute of Technology (CIT)
Tsudanuma 2-17-1, Narashino, Chiba 275-0016, Japan

Supporting information for this article is given via a link at the end of the document.

Abstract: Light-emitting systems using an RNA aptamer−dye pair, such as Spinach RNA, are an attractive method for imaging and tracing RNA expression *in vitro* and *in vivo*. We present an alternative Spinach method by genetic alphabet expansion using an unnatural base pair system, in which a dye-conjugated unnatural base substrate is site-specifically incorporated at a specific position in Spinach RNA by transcription involving the third base pair. The incorporation position was predicted by molecular dynamics simulations. This dye-conjugated Spinach RNA increased the thermal stability of the fluorescence, the robustness against ion sensitivity, and the resistance against photobleaching. Furthermore, we applied our method to Baby Spinach, a shorter version of Spinach, for dye conjugation toward the visible detection of transcripts. This is the first demonstration of an alternative RNA imaging method for a detection system using genetic alphabet expansion.

Introduction

Fluorescence imaging of specific RNAs is essential for gene expression and functional RNA analyses *in vivo* and *in vitro*, and various RNA imaging techniques have been developed.[1] One of the approaches is RNA mimics of green fluorescent protein (GFP), using light-emitting RNA aptamers such as Spinach, Mango, and Broccoli.[2] These fluorophore-targeting RNA aptamers were generated by *in vitro* selection or SELEX (Systematic Evolution of Ligands by Exponential Enrichment).[3] The fluorophores bind specifically to the RNA aptamers and increase their fluorescence. One of the fluorophores, 3,5-difluoro-4-hydroxybenzylidene (DFHBI), emits fluorescence upon binding to a specific site in the tertiary structure of Spinach RNA, enabling live-cell RNA imaging by tagging the Spinach RNA gene to a target RNA gene. Many studies have reported variants and improved methods with combinations of light-emitting RNA aptamers and fluorophores.[4]

RNA imaging methods based on light-up RNA aptamer and dye pairs have also been widely applied to various biosensor applications. For example, binary light-up aptameric sensors would be an economical alternative to detect nucleic acid targets, as compared to the conventional molecular beacon strategy[5] and could also be expressed in cells for intracellular monitoring of biological molecules[6]. Recently, one of the fluorescent aptamers, Broccoli, with the binding dye, DFHBI-1T, was applied to the detection of water contaminants.[7] In the system, ROSALIND (RNA Output Sensors Activated by Ligand Induction), *in vitro* transcription is triggered by the binding of target biomarkers with allosteric transcription factors, producing the fluorescent aptamer transcript with DFHBI-1T for visual detection.

The affinity of the Spinach RNA to DFHBI is relatively low (K_d = 537 nM) and depends on the environmental conditions, such as temperature and metal ion concentrations,[2a] and thus an excess amount of DFHBI is required for practical use.[8] One of the serious issues is the light-induced photobleaching caused by the *cis-trans* isomerisation of DFHBI in the complex with the Spinach RNA.[9] To address this issue, modified DFHBI systems for increased photostability and enhanced fluorophore recycling have been investigated.[10]

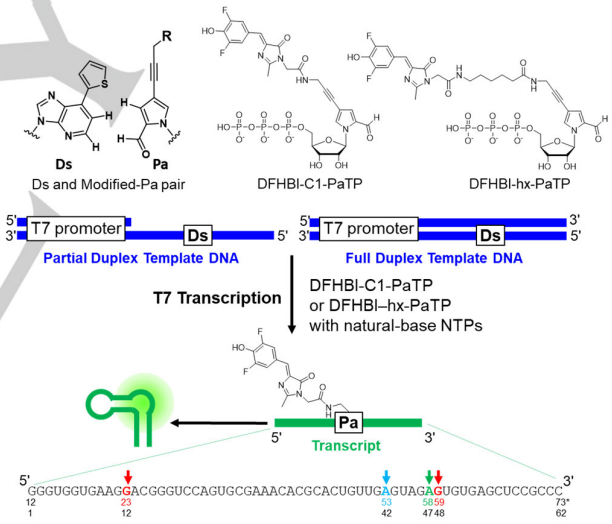

Figure 1. Chemical structures of the Ds−Pa pair, DFHBI-C1-PaTP, and DFHBI-hx-PaTP, and scheme of the T7 RNA transcription for the incorporation of the DFHBI-conjugated Pa at specific positions (indicated by arrows: G23, A53, A58, and G59) in the Spinach RNA. We use the base numbering according to the original 84-mer Spinach RNA (Figure 2A), although this full-length transcript is 62-mer.

To address this affinity-stability issue, we now report another light-up RNA approach, in which a fluorophore-conjugated nucleotide is directly incorporated at a specific position in the Spinach RNA by transcription. Genetic alphabet expansion[11] enables this specific incorporation of the fluorophore-conjugated nucleotide into a desired position of the light-up RNA, using an unnatural base pair (UBP), Ds−Pa (Figure 1).[12] T7 RNA polymerase (T7RNP) and its variants incorporate the triphosphate substrates of Pa and

modified Pa bases at the specific position in the RNA opposite Ds in DNA templates.[13]

We now report the *in vitro* site-specific incorporation of DFHBI-conjugated Pa substrates into Spinach RNA by T7RNP and the examinations of the fluorescent properties of the transcripts. We chemically synthesised two types of ribonucleoside triphosphates of DFHBI-conjugated Pa, with different linker lengths (DFHBI-C1-PaTP and DFHBI-hx-PaTP) (Figure 1). The incorporation site of these substrates was predicted and assessed by molecular dynamics (MD) simulations. The Spinach RNA containing the DFHBI-Pa base at a specific position efficiently and robustly emitted fluorescence. In addition, this covalent fluorophore-Spinach system improved the stability against light-induced photobleaching, as compared to the conventional Spinach RNA and DFHBI pair. Furthermore, we developed shorter Spinach RNAs, modified Baby2 and mBaby2,[8b, 14] for the DFHBI-conjugated Pa incorporation and demonstrated the efficient visual detection of the T7 transcription. The results provide valuable information toward *in vitro* detection and *in vivo* imaging systems using genetic alphabet expansion.

Results and Discussion

Design and preparation of DFHBI-conjugated Pa

First, we determined the DFHBI-Pa incorporation site in the Spinach RNA by RNA modeling and MD simulations, based on the tertiary structure of the RNA-DFHBI complex. For the modeling, we designed two types of DFHBI-conjugated Pa bases with different linkers (DFHBI-C1-Pa and DFHBI-hx-Pa) (Figure 1). Based on the tertiary structure of the Spinach RNA complexed with DFHBI, we considered that the replacement of A58 with Pa would allow DFHBI conjugation via a linker (Figure 2A). In our research, we use the base numbering, such as A58, according to the original 84-mer Spinach sequence[15] (Figure 2A). The MD simulations based on the monitored dihedral angles indicated the stable structures of the models, in which either DFHBI-C1-Pa or DFHBI-hx-Pa is located at position 58. In the models, the DFHBI moieties both settled in the DFHBI binding pocket of the original Spinach RNA aptamer (Figure 2A). In the simulations, only the linker parts, especially in DFHBI-hx-Pa, appreciably moved (Figure 2B). Furthermore, the DFHBI-Pa incorporation at A58 did not cause large fluctuations in the core motif located between two stem regions (blue and purple regions in Figure 2A), which tended to fluctuate more during the 10-ns simulation time (Figures 2C and S1).

Chemical synthesis of DFHBI-conjugated PaTPs

The MD simulations encouraged us to chemically synthesise the triphosphate derivatives of both DFHBI-C1-PaTP and DFHBI-hx-PaTP, which were prepared by conjugating the NHS ester of DFHBI with NH_2-C1-PaTP and NH_2-hx-PaTP, respectively (Scheme S1). The products were purified by C18-HPLC and characterised by ^1H and ^{31}P NMR and ESI-MS (Figures S2B to S2G). The molar absorption coefficients of DFHBI-C1-PaTP and DFHBI-hx-PaTP were 29,000 $M^{-1}cm^{-1}$ at 420 nm and 28,000 $M^{-1}cm^{-1}$ at 422 nm, respectively (Figure S2A). No significant fluorescence from the triphosphates in buffer was observed (Figure S3). The quantum yields of both DFHBI-C1-PaTP and DFHBI-hx-PaTP (0.0007) were similar to that of DFHBI.

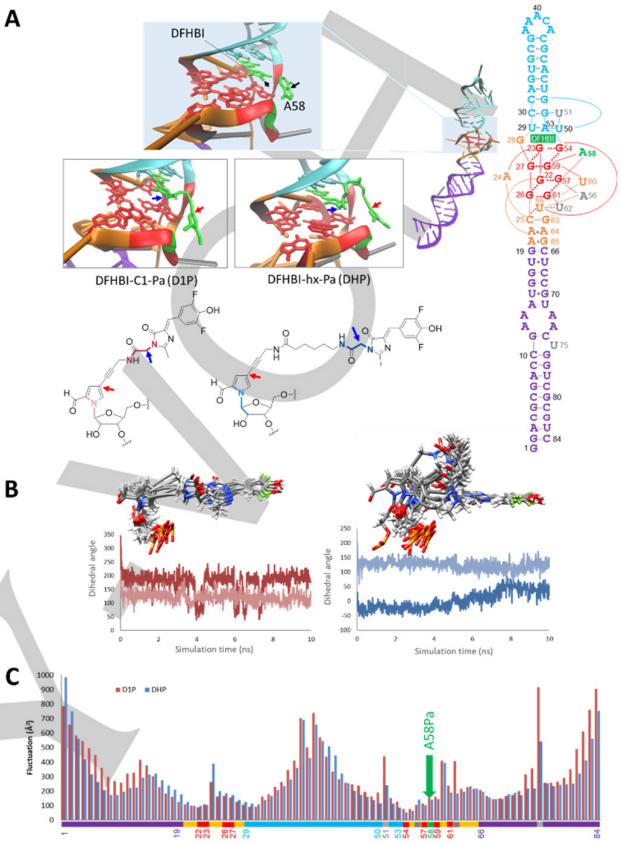

Figure 2. Molecular dynamics (MD) simulation of Spinach RNA with DFHBI-conjugated Pa at position 58A. **A**. Model building by replacing A58 and DFHBI with the DFHBI-conjugated Pa bases with different linkers (D1P in DFHBI-C1-Pa and DHP in DFHBI-hx-Pa). The connection positions for each linker are indicated by the red and blue arrows. **B**. Plots of the dihedral angles for the colored chemical bonds (light and dark brown for D1P, light and dark blue for DHP) against the 10-ns simulation time. The light and dark plots are for the glycoside bonds and the junction between DFHBI and the amide, respectively. Ten structures of D1P and DHP, chosen at each 1 ns, are superimposed. **C**. Plot of fluctuations at each nucleotide position for D1P (brown) and DHP (blue) during the MD simulation. The color patterns correspond to those shown in the secondary structures in **A**.

T7 transcription for the DFHBI-conjugated Pa incorporation

T7 transcription was performed by incubating 1 μM partially or fully double-stranded Ds-containing DNA templates (Figure 1 and Table S1), 1 mM natural-base NTPs, and 0, 0.5 or 1 mM DFHBI-PaTP (C1 or hx) at 37°C for 3 h, using T7RNP. In the partially double-stranded DNA templates, only the T7 promoter region is duplexed. The Ds-containing DNA templates (80-mer) contained two 2'-*O*-methyl nucleosides at the 5'-termini, to reduce the non-template extension of the transcribed RNAs.[16] Full-length transcripts (62-mer) containing DFHBI-C1-Pa or DFHBI-hx-Pa at position 23 (G23Pa), 53 (A53Pa), 58 (A58Pa) or 59 (G59Pa) (the numbering used in the literature[15], Figure 1) and the control

transcript (WT) using a DNA template with only the natural bases, were analysed and purified by gel-electrophoresis (Figures 3, 4, and S4). Positions 23, 53 and 59, which are close to position 58 and the DFHBI binding site (Figure 1), were chosen as controls to validate the effectiveness of position 58 for DFHBI-conjugated Pa incorporation.

Figure 3. T7 transcription using the conventional Spinach RNA templates

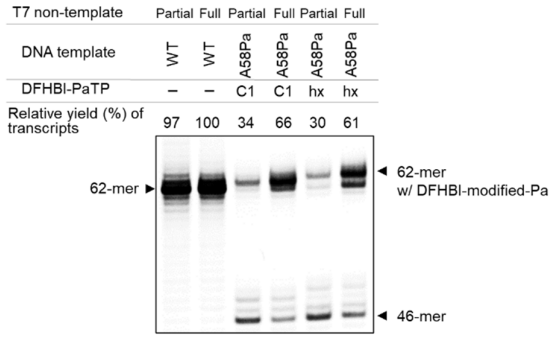

(WT) and Ds-containing DNA templates for A58Pa with DFHBI-C1- and DFHBI-hx-PaTP (1 mM). After an incubation at 37°C for 3 h, transcripts were analysed on a 7 M urea-polyacrylamide gel. The relative yields (%) were calculated by normalising the full-length transcript (62-mer) band densities based on that of the WT transcription using the fully double-stranded DNA template.

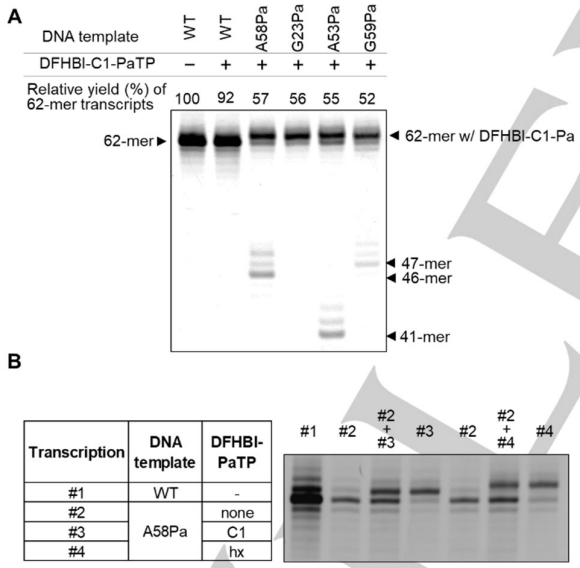

Transcription	DNA template	DFHBI-PaTP
#1	WT	-
#2	A58Pa	none
#3		C1
#4		hx

Figure 4. T7 transcription involving the DFHBI-Pa and Ds pairing. **A**. Band patterns of the transcripts from each Ds-containing DNA template for the A58Pa, G23Pa, A53Pa, and G59Pa transcripts and the WT template in the presence and absence of DFHBI-C1-PaTP (1 mM), on a 7 M urea-polyacrylamide gel. The relative yields of the full-length transcripts (62-mer) were determined based on the WT transcription in the absence of DFHBI-C1-PaTP. **B**. Band patterns of full-length transcripts. The transcription reactions with or without each DFHBI-PaTP (#1–#4) and mixtures of the solutions (#2 with #3 or #4) were analysed on a longer denaturing gel.

The transcription efficiencies involving the DFHBI-Pa incorporation using the fully double-stranded DNA templates were higher than those using the partially double-stranded ones, which were around 60% when using the fully double-stranded templates, as compared to the WT transcription (Figures 3, 4, and S4). The results were consistent with our previous observations (~50% of transcription efficiency) for the incorporations of large fluorophore-conjugated Pa substrates, such as TAMRA-hx-Pa and Cy3-PaTP, using the Ds–Pa pair system.[13c]

There were no significant differences in the transcription efficiencies between the linkers, C1 and hx, for the DFHBI-Pa substrates at position 58. The transcription slightly paused around the -1 position of each UB (corresponding to 46-mers in Figure 3 and 41- and 46/47-mers in Figures 4A and S4). The transcription with the fully double-stranded templates reduced the pausing at the unnatural base positions, relative to that with the partially double-stranded templates (Figure 3A). The full-length transcripts containing DFHBI-Pa ran slowly on the gel, as compared to the mobility of WT. This mobility shift difference confirmed the predominant DFHBI-Pa incorporation. In the presence of DFHBI-PaTP, most of the full-length transcripts were shifted on the gel (#3 and #4 in Figure 4B). In contrast, in the absence of DFHBI-PaTP, the transcription using the Ds-containing DNA templates produced full-length transcripts by the natural-base misincorporation opposite Ds in the templates (#2 in Figure 4B). Thus, the DFHBI-Pa substrates prevented the natural-base misincorporation and were predominantly incorporated into RNA opposite Ds.

The transcription reactions using the WT template in the presence of DFHBI-PaTP generated similar band patterns to those of the transcripts in the absence of DFHBI-PaTP (Figures 4A and S4), indicating the rare misincorporation of DFHBI-Pa opposite natural bases. Due to the high efficiency of the WT transcription, additional nucleotide insertions (+1 and +2 WT-transcript bands) were slightly observed by non-templated incorporation (Figures 3, 4, and S4).

The excitation and emission spectra of A58Pa RNA containing DFHBI-Pa (C1 or hx) were obtained (Ex: 461 nm, Em: 503 nm for C1, Ex: 472 nm, Em: 507 nm for hx, Figure S3).

Characterisation of the transcripts containing DFHBI-Pa

We tested the specific fluorescence light-emission of these transcripts. The fluorescence of each gel-purified, full-length transcript was analysed on a native gel, and the fluorescence intensities of each transcript solution were measured with a plate reader (Excitation: 461 nm, Emission: 501 nm) (Figure 5A for the DFHBI-hx-Pa incorporation and Figure S5 for the DFHBI-C1-Pa incorporation). For the WT transcript (conventional Spinach RNA), the fluorescence intensities were measured in the presence of an equal amount (0.1 μM) of DFHBI (WT-DFHBI pair).

As predicted by the MD simulations, only the A58Pa transcripts containing both DFHBI-C1-Pa and DFHBI-hx-Pa exhibited strong fluorescence intensities. The WT transcripts obtained by T7 transcription in the presence of DFHBI-PaTPs had no fluorescence (Figures 5A and S5). These results confirm that the specific incorporation of DFHBI-PaTPs opposite position 58 provides strong fluorescence emission.

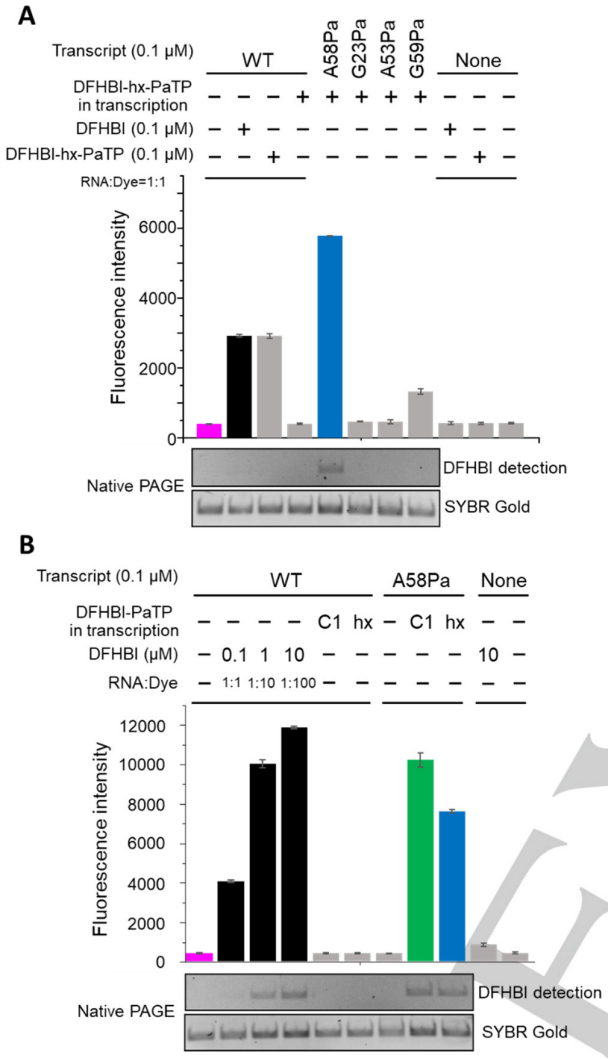

Figure 5. Fluorescence intensities of the transcripts containing DFHBI-Pa and the conventional Spinach RNA (WT) and DFHBI complex. **A**. Fluorescence intensities of the transcripts containing DFHBI-hx-Pa at specific positions and the WT transcript, in the presence and absence of DFHBI or DFHBI-hx-PaTP. Fluorescence was measured at 503 nm (ex. 461 nm) in a buffer solution. The transcripts were also analysed by detecting the DFHBI fluorescence (at 510 nm, before staining) and staining the native gel with SYBR Gold. **B**. Fluorescence intensities of A58Pa (DFHBI-C1 and DFHBI-hx) and WT transcripts.

The quantum yields of the A58Pa (DFHBI-C1 and DFHBI-hx) transcripts were 0.51 and 0.58, respectively, and that of the WT-DFHBI complex was 0.72[4c] (Figure S3C). Despite the lower quantum yields of the A58Pa transcripts than that of WT-DFHBI, their fluorescence intensities in solution were around two-fold higher than that of WT with 0.1 μM DFHBI (1:1 molar ratio) (Figures 5A and S5). The G59Pa transcript was also slightly fluorescent. Position 23 is located at the site opposite position 58 in the tertiary structure of the Spinach RNA. However, no fluorescence from the G23Pa and A53Pa transcript was observed. These results indicate the importance of the DFHBI-Pa incorporation at a specific position in the Spinach RNA, for the formation of the RNA aptamer and DFHBI complex.

The fluorescence of the A58Pa transcript was also observed on the native gel (Figure 5). In contrast, the fluorescence of the 1:1 molar ratio of WT and DFHBI was not visible on the gel. These results suggested that the direct incorporation of DFHBI at the specific position in the Spinach RNA efficiently stabilises the DFHBI-binding complex on the gel. With increasing DFHBI concentrations, the fluorescence of WT with 1 μM or 10 μM DFHBI (1:10 or 1:100 molar ratio, respectively) was observed on the gel (Figure 5B). In the solution, the fluorescence intensity of A58Pa is comparable to that of WT in the presence of 1 μM DFHBI (the ratio between WT and DFHBI was 1:10).

The fluorescence intensity of the A58Pa transcript containing DFHBI-C1-Pa was slightly higher than that containing DFHBI-hx-Pa and as high as that of WT with 1 μM DFHBI (Figure 5B). The MD simulation indicated that the hexyl linker moiety of DFHBI-hx-Pa is highly flexible (Figure 2B), thus reducing the stability of the DFHBI moiety in the binding complex.

Interestingly, the fluorescence intensity of WT in the presence of DFHBI-hx-PaTP was as high as that of the WT-DFHBI (1:1) pair (Figure 5A). In contrast, the fluorescence intensity of DFHBI-C1-PaTP with the shorter linker was lower than that of the WT-DFHBI (1:1) pair (Figure S5). Thus, the longer hexyl linker facilitates the insertion of the DFHBI moiety into the binding site of the WT Spinach RNA.

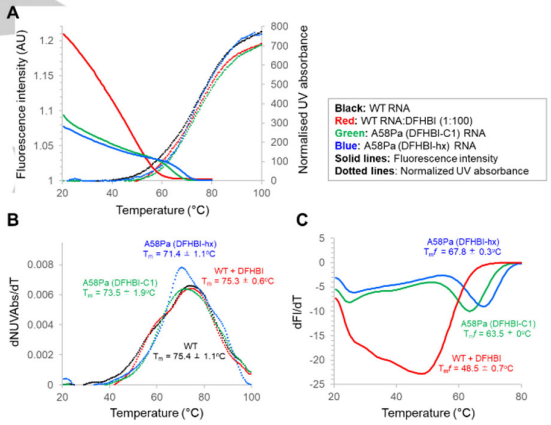

Figure 6. Temperature dependencies of the structural stabilities and fluorescence intensities of each transcript. (a) Temperature-dependent melting profiles, measured by the fluorescence intensity and UV absorbance at 260 nm. Fluorescence intensities were measured at 503 nm (ex. 461 nm), and UV absorbance was measured at 260 nm, with 2.5 μM of each RNA for UV absorbance and 100 nM of each RNA for fluorescence (with 10 μM of DFHBI for WT). (b) First derivatives of the UV absorbance melting profiles of each transcript. (c) First derivatives of the fluorescence intensity melting profile of each transcript.

Since the gel analysis indicated the robust stability and fluorescence of the A58Pa transcripts, we assessed their thermal stabilities by measuring the temperature-dependent melting profiles of the fluorescence emission (T_mf) and UV absorbance (T_m) (Figure 6).[17] As a control, to observe the clear fluorescence of the WT transcript, we added a 100-fold excess of DFHBI. The thermal stabilities of the tertiary

structures of each transcript were similar among A58Pa (DFHBI-C1), A58Pa (DFHBI-hx), WT, and WT-DFHBI (Figure 6A), and the T_m values were 73.5 ± 1.9, 71.4 ± 1.1, 75.4 ± 1.1, and 75.3 ± 0.6˚C, respectively (Figure 6B). In contrast, the fluorescence of both A58Pa (DFHBI-C1) and A58Pa (DFHBI-hx) was highly resistant to the temperature change, as compared to that of the WT-DFHBI complex (Figure 6A and 6C). With the addition of a 100-fold excess amount of DFHBI to the WT solution, the WT-DFHBI complex exhibited high fluorescence at low temperature. However, the T_mf value of the complex (48.5 ± 0.7˚C) was significantly lower than those of A58Pa (DFHBI-C1) and A58Pa (DFHBI-hx) (63.5 ± 0.0 and 67.8 ± 0.3˚C, respectively) (Figure 6C).

As the MD simulation indicated, the T_m value of A58Pa (DFHBI-hx) was also slightly lower than those of A58Pa (DFHBI-C1) and WT-DFHBI. However, the T_mf value of A58Pa (DFHBI-hx) was higher than that of A58Pa (DFHBI-C1). One possible explanation is the flexibility of the DFHBI-hx-Pa in the complex. During the thermal denaturation of the RNA structure, the DFHBI moiety might remain in the binding pocket, due to the flexibility of the hexyl linker moiety. At temperatures up to 60˚C, the A58Pa (DFHBI-C1) and (DFHBI-hx) transcripts both exhibited high fluorescence intensities.

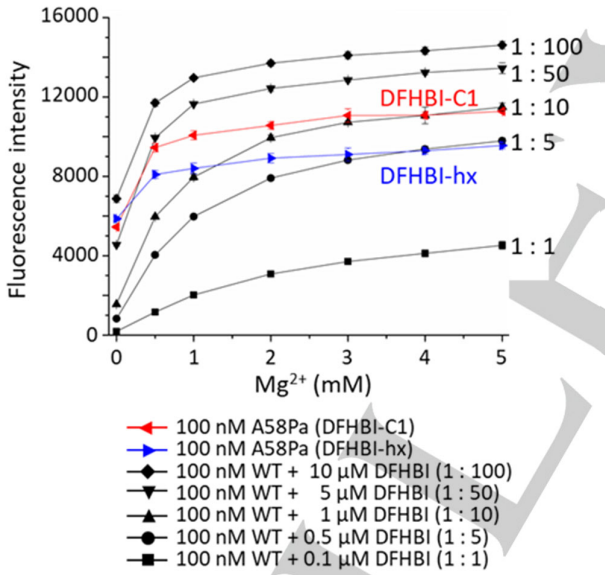

Figure 7. Magnesium ion dependency of the fluorescence intensities of A58Pa (DFHBI-C1 and DFHBI-hx) and the WT−DFHBI complexes. The fluorescence was measured at 507 nm (ex. 472 nm) in buffer containing different Mg^{2+} concentrations (0−5 mM).

One issue with the conventional Spinach RNA is the strong dependence on metal ions.[2a, 15, 18] In particular, at a Spinach RNA (WT) and DFHBI ratio lower than 1:10, the fluorescence intensity significantly decreases in a solution containing less than 1 mM Mg^{2+} (Figures 7 and S6). In contrast, the fluorescence of the A58Pa transcripts without Mg^{2+} was as high as that of the WT-DFHBI complex at the 1:50 ratio and strong intensities were maintained at Mg^{2+} concentrations higher than 0.5 mM (Figure 7). At high Mg^{2+} concentrations (4–5 mM), the fluorescence intensities of A58Pa (DFHBI-C1) and (DFHBI-hx) were comparable to those of the respective 1:10 and 1:5 ratios of the WT-DFHBI complexes.

Another issue with the conventional Spinach RNA–DFHBI pair is the photobleaching by the *cis-trans* isomerisation of DFHBI induced by continuous irradiation.[9] Encouraged by the robust stability of the core moiety in the DFHBI-conjugated A58Pa (DFHBI-C1 and DFHBI-hx) transcripts, we examined the *in vitro* photostabilities of the A58Pa transcripts, as well as the WT RNA with DFHBI or DFHBI-hx-PaTP, using a cuvette-based irradiation method[10] (Figure 8). DFHBI-hx-PaTP also binds to the WT RNA and exhibits fluorescence emission (Figure 5A) and thus is a suitable control to evaluate the photostability of the dye-conjugated Pa unit. The initial (within 5 sec) fluorescence reductions of the A58Pa (DFHBI-C1 and DFHBI-hx) transcripts, as well as the WT RNA–DFHBI-hx-PaTP pair, were around 2-fold slower than that of the WT–DFHBI pair (the left side panel in Figure 8), suggesting the increased photostability of the DFHBI conjugation to Pa with the linker against *cis→trans* isomerisation. In contrast, upon irradiation for longer period (within 600 sec), the WT complexes with both DFHBI-hx-PaTP and DFHBI showed lower plateaus than those of the A58Pa (DFHBI-C1 and DFHBI-hx) transcripts (right panel in Figure 8). These results indicated that the DFHBI conjugation with Spinach RNA might facilitate the rebinding of the conjugated *cis* isomer of the DFHBI moiety, after reverse *trans→cis* isomerisation. Overall, the photostability of the DFHBI-conjugated Spinach RNAs was improved by two effects: reducing the light-induced *cis→trans* isomerisation in the dye-binding site (originated in the chemical structure modification via linker attachment to DFHBI) and increasing the binding affinity of the *cis* isomer of DFHBI (probably k_{on} increase via direct RNA conjugation).

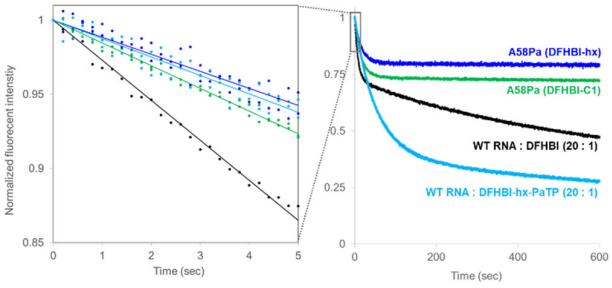

Figure 8. *In vitro* photostability of A58Pa transcripts (DFHBI-C1 and DFHBI-hx, 100 nM) and the WT RNA-DFHBI complexes (2 µM WT RNA with 100 nM DFHBI or DFHBI-hx-PaTP). The fluorescence was measured at 505 nm (ex. 461 nm).

Miniaturisation of Spinach RNA

Given the stabilisation of our dye-conjugated Spinach method, it might be possible to shorten the length of the Spinach RNA. Shorter versions of Spinach RNA, Baby (52-mer) and mBaby (44-mer) Spinach, were obtained by miniaturising the original one (62-mer) (Figure 9).[14] However,

these shorter versions of Spinach RNA suffered from relatively poor folding efficiency and consequently exhibited lower fluorescence intensity.[8b] Therefore, we also designed their stabilised versions, Baby2 (53-mer) and mBaby2 (47-mer), by introducing G–C pairs into their stem regions (Figure 9).

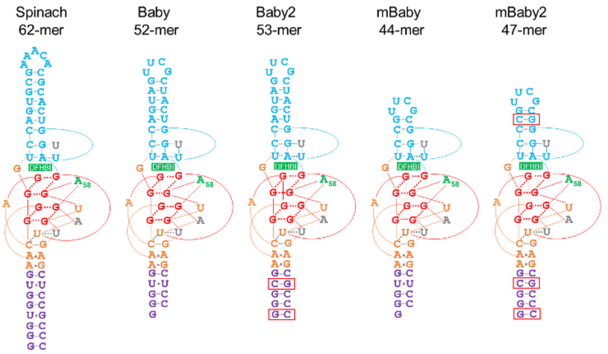

Figure 9. Predicted secondary structures of the original, Baby, and mBaby Spinach RNAs, as well as Baby2 and mBaby2 stabilised by introducing G–C pairs in the stem regions (enclosed in red boxes). The DFHBI-Pa incorporation sites are indicated in green.

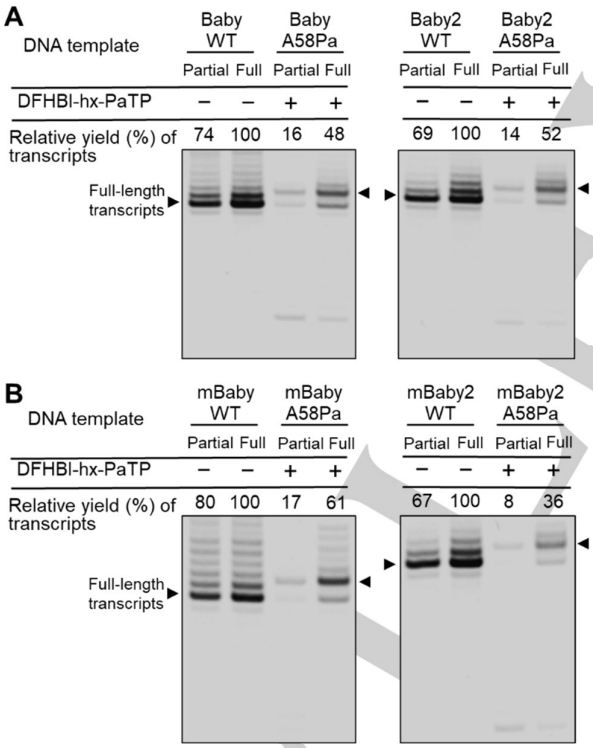

Figure 10. Analysis of transcripts of the shorter versions, Baby, Baby2, mBaby, and mBaby 2 for WT and A58Pa (DFHBI-hx-Pa, 1 mM), after 3-hour T7 transcription reactions using fully or partially double-stranded DNA templates.

The transcription was performed using 1 μM of each fully or partially double-stranded template in the presence or absence of 1 mM DFHBI-hx-PaTP. The transcription efficiencies of A58Pa for Baby, Baby2, mBaby, and mBaby2 were 48–61% when using the fully double-stranded templates, as compared with those of WT (Figure 10). Partially double-stranded templates, especially for mBaby2, significantly reduced the transcription efficiencies. This might be due to secondary structure formation in the single-stranded regions in the templates.

The stabilised Baby2 and mBaby2 transcripts for both WT (RNA/DFHBI = 1:10) and A58Pa exhibited high fluorescence intensities (Figure 11). Both the WT and A58Pa mBaby transcripts with DFHBI were fluorescently inactive. In contrast, the Baby A58Pa showed high fluorescence emission, although the original WT Baby was inactive. Thus, the conjugation of DFHBI to Baby Spinach stabilises the tertiary structure for the appropriate localisation of DFHBI, and mBaby2 can be used as the shortest version of Spinach RNA with high emission.

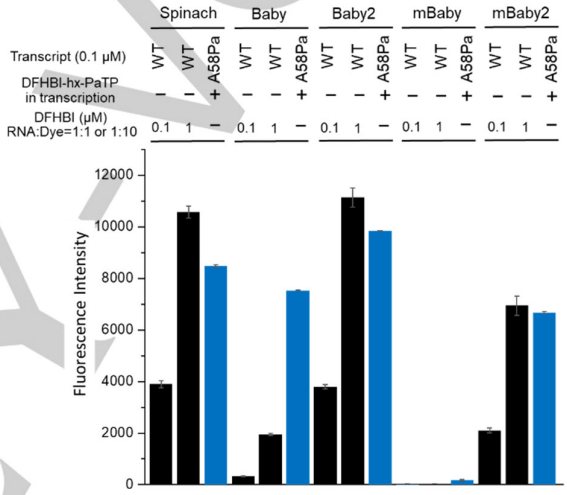

Figure 11. Fluorescence intensities of the WT transcripts in the presence of DFHBI (1- or 10-fold) and the A58Pa transcripts containing DFHBI-hx-Pa at position 58, for the original Spinach, Baby, Baby2, mBaby, and mBaby2. Fluorescence was measured at 503 nm (Ex. 461 nm).

Real-time monitoring and visualisation of T7 transcription

In vitro transcription monitoring using light-emitting RNA aptamers provides various biosensor applications, such as a cell-free biosensor to detect water contaminants in low-resource settings[7]. Thus, we examined the utility of our method for such monitoring applications. We performed real-time fluorescent tracing and visualisation of transcripts in *in vitro* T7 transcription reactions, by the site-specific DFHBI-Pa incorporation system using the fully double-stranded A58Pa DNA templates for 62-mer Spinach (SpA58Pa) and 53-mer Baby2 (Baby2 A58Pa) in the presence of 0.5 mM DFHBI-hx-PaTP and 1 mM natural base NTPs. As a control, the WT Spinach (SpWT) and Baby2 (Baby2 WT) transcriptions were also performed in the presence of 10 μM DFHBI. The fluorescence intensities in the reactions were continuously monitored at 507 nm (ex. 472 nm) at 37°C for 4 h.

The transcription was successfully monitored by the DFHBI-hx-Pa incorporation into A58Pa (Figure 12A). The transcription using the shorter version, Baby2 A58Pa, exhibited higher sensitivity, as compared to the Baby2 WT transcription with 10 μM

of DFHBI, and the fluorescence of the Baby2 A58Pa transcription was visually detected and as high as those of the SpA58Pa and SpWT transcriptions (Figure 12B). Even in a 1 h transcription reaction, the fluorescence was sufficiently detectable (Figure 12C). The Baby2 A58Pa transcripts probably folded more easily in transcription, as compared to the Baby2 WT transcripts. The fluorescence intensity of the SpWT–DFHBI pair was reduced by longer irradiation periods (black solid line in Figure 12A). This might be due to photobleaching of the system and less-efficient DFHBI *cis*-isomer recycling in the large amounts of transcript, as shown in Figure 8. Thus, the method using DFHBI-PaTP provides a highly stable detection system for the light-up aptamers as the output signal of cell-free biosensors.

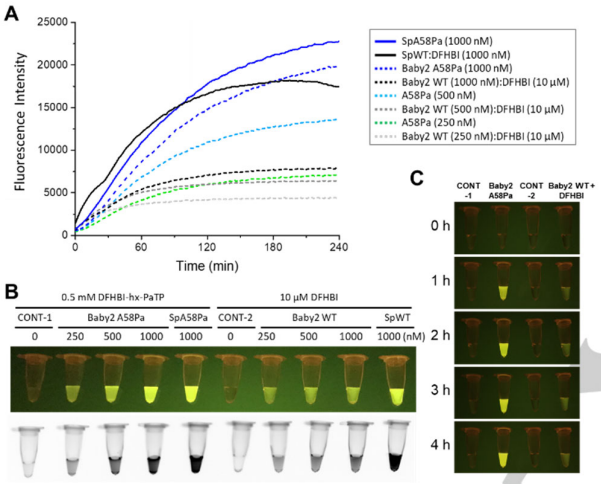

Figure 12. Real-time monitoring and visualisation of *in vitro* transcription. The fluorescence intensity during transcription with various template concentrations (250–1,000 nM) was monitored (excitation 461 nm, emission 503 nm) (**A**). In the T7 transcription, 0.5 mM DFHBI-hx-PaTP for A58Pa or 10 μM DFHBI for WT were used for monitoring. The fluorescence of each transcription reaction after 4 h (**B**) or each hour with 1000 nM template (**C**) was visually detected with a Blue LED transilluminator. Cont-1 and Cont-2 present transcriptions without templates in the presence of 0.5 mM DFHBI-hx-PaTP and 10 μM DFHBI, respectively.

Conclusion

We have demonstrated an RNA light-emitting method using genetic alphabet expansion technology, as an alternative to the conventional RNA/dye pair method. In T7 transcription, DFHBI-conjugated PaTP was site-specifically incorporated into Spinach transcripts opposite Ds in the DNA templates, and the efficient light-emission by the transcripts was observed. The incorporation site of DFHBI-Pa was correctly assessed by MD simulations. The fluorescence of the DFHBI-Pa-containing RNAs was thermally stable and tolerated a wide range of Mg^{2+} concentrations, as compared to the conventional Spinach system, enabling the design of a shorter version of the Spinach RNA. Thus, the dye-conjugated Spinach method by genetic alphabet expansion can be used for highly sensitive monitoring and visualisation.

This dye-conjugated Spinach RNA increased the stability against photobleaching by two factors: the stabilisation of the *cis-trans* photoisomerisation and the improved rebinding of the reproduced *cis* isomer of the DFHBI moiety. Other modifications of DFHBI, such as BI and DFNS, with Broccoli RNA reportedly resist the *cis–trans* photoisomerisation and increase the recycling.[10] Thus, our method could be further improved by the BI- or DFNS-conjugated Pa incorporation to the Broccoli system.

As for *in vivo* imaging, this is the first step toward the development of a new type of Spinach RNA conjugated DFHBI. In the system, the shorter Spinach RNA might be useful for its conjugation with target gene transcripts. Similar to the DFHBI addition in the conventional Spinach method, our system also requires the DFHBI-conjugated substrate, which might increase the background fluorescence in *in vivo*. The background signals result from the nonspecific interactions of the dye materials with cellular components and the high viscosity in the cell. This background issue could be improved by using FRET systems.[8a, 19] Romesberg's team has already developed semi-synthetic organisms using their unnatural base pairs, which function in *in vivo* replication, transcription, and translation.[20] Therefore, it is highly possible that *in vivo* imaging can be achieved using this genetic alphabet expansion system.

Experimental Section

Refer to Supplementary Information

Acknowledgement

This work was supported by the Institute of Bioengineering and Bioimaging (Biomedical Research Council, Agency for Science, Technology and Research, Singapore).

Keywords: Spinach RNA • Genetic Alphabet Expansion • Unnatural Base Pair • Transcription • Aptamer

References

[1] a) H. Sato, S. Das, R. H. Singer and M. Vera, *Annu. Rev. Biochem.* **2020**; b) S. Yoon and J. J. Rossi, *Pharmaceuticals (Basel)* **2018**, *11*, 71; c) D. Gemmill, S. D'Souza, V. Meier-Stephenson and T. R. Patel, *Biochem. Cell Biol.* **2020**, *98*, 31-41; d) B. Y. Michel, D. Dziuba, R. Benhida, A. P. Demchenko and A. Burger, *Front. Chem.* **2020**, *8*, 112; e) J. T. George and S. G. Srivatsan, *Methods* **2017**, *120*, 28-38; f) E. Tutucci, N. M. Livingston, R. H. Singer and B. Wu, *Annu. Rev. Biophys.* **2018**, *47*, 85-106; g) T. P. Constantin, G. L. Silva, K. L. Robertson, T. P. Hamilton, K. Fague, A. S. Waggoner and B. A. Armitage, *Org. Lett.* **2008**, *10*, 1561-1564.
[2] a) J. S. Paige, K. Y. Wu and S. R. Jaffrey, *Science* **2011**, *333*, 642-646; b) E. V. Dolgosheina, S. C. Jeng, S. S. Panchapakesan, R. Cojocaru, P. S. Chen, P. D. Wilson, N. Hawkins, P. A. Wiggins and P. J. Unrau, *ACS Chem. Biol.* **2014**, *9*, 2412-2420; c) G. S. Filonov, J. D. Moon, N. Svensen and S. R. Jaffrey, *J. Am. Chem. Soc.* **2014**, *136*, 16299-16308; d) J. Ouellet, *Front. Chem.* **2016**, *4*, 29; e) A. Autour, S. C. Y. Jeng, A. D. Cawte, A. Abdolahzadeh, A. Galli, S. S. S. Panchapakesan, D. Rueda, M. Ryckelynck and P. J. Unrau, *Nat. Commun.* **2018**, *9*, 656.
[3] a) A. D. Ellington and J. W. Szostak, *Nature* **1990**, *346*, 818-822; b) C. Tuerk and L. Gold, *Science* **1990**, *249*, 505-510.

[4] a) R. L. Strack, M. D. Disney and S. R. Jaffrey, *Nat. Methods* **2013**, *10*, 1219-1224; b) X. Chen, D. Zhang, N. Su, B. Bao, X. Xie, F. Zuo, L. Yang, H. Wang, L. Jiang, Q. Lin, M. Fang, N. Li, X. Hua, Z. Chen, C. Bao, J. Xu, W. Du, L. Zhang, Y. Zhao, L. Zhu, J. Loscalzo and Y. Yang, *Nat. Biotechnol.* **2019**, *37*, 1287-1293; c) W. Song, R. L. Strack, N. Svensen and S. R. Jaffrey, *J. Am. Chem. Soc.* **2014**, *136*, 1198-11201; d) A. Autour, E. Westhof and M. Ryckelynck, *Nucleic Acids Res.* **2016**, *44*, 2491-2500; e) K. D. Warner, L. Sjekloca, W. Song, G. S. Filonov, S. R. Jaffrey and A. R. Ferre-D'Amare, *Nat. Chem. Biol.* **2017**, *13*, 1195-1201; f) G. S. Filonov, W. Song and S. R. Jaffrey, *Biochemistry* **2019**, *58*, 1560-1564.

[5] a) D. M. Kolpashchikov and A. A. Spelkov, *Angew Chem Int Ed Engl* **2021**, *60*, 4988-4999; b) E. B. Porter, J. T. Polaski, M. M. Morck and R. T. Batey, *Nat. Chem. Biol.* **2017**, *13*, 295-301.

[6] a) C. A. Kellenberger, Z. F. Hallberg and M. C. Hammond, *Methods Mol Biol* **2015**, *1316*, 87-103; b) J. L. Litke, M. You and S. R. Jaffrey, *Methods Enzymol* **2016**, *572*, 315-333.

[7] J. K. Jung, K. K. Alam, M. S. Verosloff, D. A. Capdevila, M. Desmau, P. R. Clauer, J. W. Lee, P. Q. Nguyen, P. A. Pasten, S. J. Matiasek, J. F. Gaillard, D. P. Giedroc, J. J. Collins and J. B. Lucks, *Nat. Biotechnol.* **2020**, *38*, 1451-1459.

[8] a) I. Shin, J. Ray, V. Gupta, M. Ilgu, J. Beasley, L. Bendickson, S. Mehanovic, G. A. Kraus and M. Nilsen-Hamilton, *Nucleic Acids Res.* **2014**, *42*, e90; b) M. Okuda, D. Fourmy and S. Yoshizawa, *Nucleic Acids Res.* **2017**, *45*, 1404-1415.

[9] a) P. Wang, J. Querard, S. Maurin, S. S. Nath, T. L. Saux, A. Gautier and L. Jullien, *Chem. Sci.* **2013**, *4*, 2865-2873; b) N. T. Dao, R. Haselsberger, M. T. Khuc, A. T. Phan, A. A. Voityuk and M. E. Michel-Beyerle, *Sci. Rep.* **2021**, *11*, 7356; c) K. Y. Han, B. J. Leslie, J. Fei, J. Zhang and T. Ha, *J. Am. Chem. Soc.* **2013**, *135*, 19033-19038.

[10] a) X. Li, H. Kim, J. L. Litke, J. Wu and S. R. Jaffrey, *Angew. Chem. Int. Ed. Engl.* **2020**, *59*, 4511-4518; b) X. Li, J. Wu and S. R. Jaffrey, *Angew. Chem. Int. Ed. Engl.* **2021**, *60*, 24153-24161.

[11] a) M. Kimoto and I. Hirao, *Chem. Soc. Rev.* **2020**, *49*, 7602-7626; b) M. Manandhar, E. Chun and F. E. Romesberg, *J. Am. Chem. Soc.* **2021**, *143*, 4859-4878; c) Z. Ouaray, S. A. Benner, M. M. Georgiadis and N. G. J. Richards, *J. Biol. Chem.* **2020**, *295*, 17046-17059.

[12] I. Hirao, M. Kimoto, T. Mitsui, T. Fujiwara, R. Kawai, A. Sato, Y. Harada and S. Yokoyama, *Nat. Methods* **2006**, *3*, 729-735.

[13] a) M. Kimoto, A. J. Meyer, I. Hirao and A. D. Ellington, *Chem. Commun.* **2017**, *53*, 12309-12312; b) T. Someya, A. Ando, M. Kimoto and I. Hirao, *Nucleic Acids Res.* **2015**, *43*, 6665-6676; c) N. Morohashi, M. Kimoto, A. Sato, R. Kawai and I. Hirao, *Molecules* **2012**, *17*, 2855-2876.

[14] K. D. Warner, M. C. Chen, W. Song, R. L. Strack, A. Thorn, S. R. Jaffrey and A. R. Ferre-D'Amare, *Nat. Struct. Mol. Biol.* **2014**, *21*, 658-663.

[15] H. Huang, N. B. Suslov, N. S. Li, S. A. Shelke, M. E. Evans, Y. Koldobskaya, P. A. Rice and J. A. Piccirilli, *Nat. Chem. Biol.* **2014**, *10*, 686-691.

[16] C. Kao, S. Rudisser and M. Zheng, *Methods* **2001**, *23*, 201-205.

[17] M. Kimoto, T. Mitsui, Y. Harada, A. Sato, S. Yokoyama and I. Hirao, *Nucleic Acids Res.* **2007**, *35*, 5360-5369.

[18] a) M. You, J. L. Litke and S. R. Jaffrey, *Proc. Natl. Acad. Sci. U S A* **2015**, *112*, E2756-E2765; b) C. L. Walker, K. A. Lukyanov, I. V. Yampolsky, A. S. Mishin, A. S. Bommarius, A. M. Duraj-Thatte, B. Azizi, L. M. Tolbert and K. M. Solntsev, *Curr. Opin. Chem. Biol.* **2015**, *27*, 64-74.

[19] M. D. E. Jepsen, S. M. Sparvath, T. B. Nielsen, A. H. Langvad, G. Grossi, K. V. Gothelf and E. S. Andersen, *Nat. Commun.* **2018**, *9*, 18.

[20] Y. Zhang, J. L. Ptacin, E. C. Fischer, H. R. Aerni, C. E. Caffaro, K. San Jose, A. W. Feldman, C. R. Turner and F. E. Romesberg, *Nature* **2017**, *551*, 644-647.

Entry for the Table of Contents

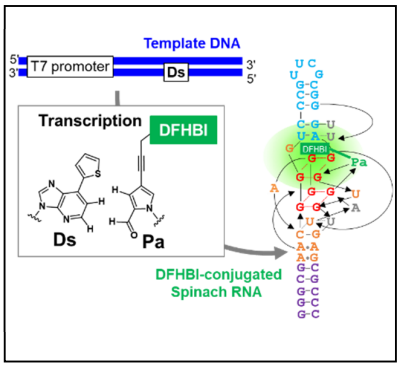

Light emission by dye-conjugated Spinach RNA transcripts generated by genetic alphabet expansion. Dye-conjugated unnatural base substrates are site-specifically incorporated into Spinach RNA opposite to its unnatural base pairing partner in DNA templates by T7 transcription. The dye-conjugated Spinach RNAs or shorter versions robustly emit fluorescence.